Research Article

Raisan F. Hamad, Ghassan F. Smaisim* and Azher M. Abed

Numerical studies of the simultaneous development of forced convective laminar flow with heat transfer inside a microtube at a uniform temperature

https://doi.org/10.1515/eng-2022-0336
received March 15, 2022; accepted June 01, 2022

Abstract: Conjugate heat transfer is a complex problem because heat is transferred from a solid medium to a liquid medium through their interfaces. The steady-state laminar flow formed inside the microtubules is subjected to a constant temperature at the outer sidewall surface. These images cover a wide range of wall-to-fluid thermal conductivity ratios (ksf = 1, 2, 3, 4, and 5) and wall thickness-to-inner diameter ratios (δ/Ri = 0.25, 0.5, 0.75, 1, 1.25, and 1.5) and Reynolds numbers (Re = 200, 400, 600, 800, and 1,000). The results are processed by a Fluent program based on the finite volume method to numerically integrate the driver's differential equations. The results show that increasing the wall-to-fluid thermal conductivity ratio ksf increases the inner wall dimensionless temperature and decreases the average Nusselt number. Conversely, an increase in the ratio of wall thickness to inner diameter results in a decrease in the dimensionless temperature of the inner wall and an increase in the average Nusselt number.

Keywords: conjugate, enhancement of heat transfer, force convection, microtube, simultaneous

*** Corresponding author: Ghassan F. Smaisim,** Department of Mechanical Engineering, Faculty of Engineering, University of Kufa, Iraq; Nanotechnology and Advanced Materials Research Unit (NAMRU), Faculty of Engineering, University of Kufa, Najaf, Iraq, e-mail: Ghassan.Smaisim@uokufa.edu.iq
Raisan F. Hamad: Department of Mechanical Engineering, Faculty of Engineering, University of Kufa, Najaf, Iraq
Azher M. Abed: Department of Air Conditioning and Refrigeration, Al-Mustaqbal University College, Babylon, Iraq

1 Introduction

Traditional hoses do not consider shafts. However, in the case of microtubules, axial conduction plays an important role in heat transfer and temperature distribution in both axial and radial directions due to the high ratio of microtubule thickness to the radius. This problem exists in many applications such as micropipes, microchannels, micro heat exchangers, micropower generation systems, and computers [1]. Microtubes are usually essential for micro-components, e.g., micronozzles, painless injection, and microexchangers. Another application are studying phase change material microchannels [2–4], Instability in flow boiling through microchannels [5], Sustainable synthetic fuel production [6], and many presentation in enhanced heat transfer from solar application fields [7–9] and nanoscience and nanotechnology applications [10,11].

Heat transfer rates and convection coefficients in liquid domains depend not only on the physical properties of the liquid but also on the physical properties of the microtubule walls surrounding the liquid. In these problems, heat is transferred through two intermediate solids and then through a liquid, which is called a conjugation problem [12].

Many researchers in the theoretical or experimental field have focused on this situation, early Barozzi and Pagliarini [13] converted the conjugate heat transfer to a fully developed laminar flow that uniformly heats the entire length of the tube. Their results examined the effect of four parameters: Peclet number, ksf, and tube aspect ratio, each taking two values. They analyzed the case using the finite element method. Celata et al. [14] heat transfer by forced convection in laminar flow microtubules. Microtubules range in diameter from 528 to 120 μm. They investigated the effects of axial conduction in the wall, viscous heating of the fluid, and thermal inlet length on the thermal behavior. The results show that the axial heat

conduction significantly affects the local Nusselt number. It also adds to its value at the air intake. Lelea et al. [15] analyzed heat transfer in microchannels and laminar flow to predict the behavior of dielectric fluids. The diameter ratio is D_i/D_o = 125.4/300 μm, the length is 70 mm, the heat flux is 0.75 W, and only part of the tube is heated. The flow characteristics of the working medium depend on the temperature. Their results predict that the local Nusselt number can have a large effect when fluid properties are a function of temperature. Zhang et al. [16] investigated the effect of axial conduction on the axial and radial laminar flow and heat transfer performance of thick-walled microtubules, and the effect of changing δsf when the wall is exposed to a uniform surface temperature. Their results show a near-constant heat flow behavior on the inner wall surface with increase in the pipe thickness and decrease in ksf. Girgin and Turker [17] developed axial laminar heat transfer in circular tubes; the numerical model is based on the finite difference method. The tube wall is exposed to constant heat flow and uniform temperature boundary conditions. Their results cover Peclet numbers from 0.5 to 100. They concluded that axial conduction effects play an important role in microtubular applications such as heat exchangers.

Elmarghany et al. [18] obtained the heat flow and temperature distribution equations (conjugate heat transfer) applied to the outer surface of a thick-walled tube. Laminar and mature flow are hydrodynamic compact thermal models. The temperature distribution inside the tube is introduced into the solid–liquid interface. Their results show that the channel wall temperature increases along the channel length. Chandel [19] numerically and experimentally investigated convective heat transfer in laminar and turbulent flow in thick-walled tubes. Reynolds numbers ranged from 454 to 13,627, and numerical results were obtained using Fluent commercial software. Their results show that as the Reynolds number increases, so does the local Nusselt number. Lin and Kandlikar [20] analyzed the effect of axial conduction on microchannel flow. They found that when the flow is fully developed, there is an increase in the axial heat transfer across all cross-sections due to increased fluid temperature. Axial conduction results in heat transfer in the wall vs fluid flow. In addition, they found that data from experiments with high precision testing was not available due to heat loss. Rahimi and Mehryar [21] studied the effect of axial wall conduction on the local Reynolds number and Nusselt number during laminar flow evolution. In this case, they performed a numerical analysis of heat transfer, applying a uniform heat flux per unit length to the outer wall surface of the tube. CFD programs are used to solve flow equation problems and heat transfer problems. Moharana et al. [22] studied the effect of axial wall conduction in conjugate heat transfer due to the formation of laminar flow and heat transfer at the bottom of the wall and all other square microchannels with uniform heat flow boundary conditions, the walls are adiabatic of ksf ≈ 0, 17–703, δ/Ri = 1–24, and Re ≈ 100–1,000. Their results suggest that ksf plays a crucial role in axial conduction. The result is very low in cases like ksf = 0. Astaraki and Tabari [23] studied forced convection heat transfer in tubes with boundary conditions as periodic functions of axial outer wall temperature. The temperature behavior of fluid and solid domains is a periodic function of the vertical direction. They analytically calculated the temperature distribution and Nusselt number in the liquid and solid range. Their results show that increasing the dimensionless frequency leads to an increase in the mean Nu number. This results in a reduction in the oscillation amplitude of the temperature field. Touahri and Boufendi [24] studied conducted convection for laminar flow in thin-walled 3D horizontal tubes. They used the second-order numerical case of the finite volume method. Their results deal with different Grashof numbers (10^4–10^7). The effects on the hydraulic and thermal zones, as well as the physical properties of the fluid, are also significant with temperature, and the average Nusselt number at the tube-solid–liquid interface increases with the Grashof number. However, you do get the relationship between the mean Nusselt number and the Richardson number. Kumar and Maharana [25] conducted a 2D numerical microtubule conjugate heat transfer with an inner radius of 0.2 mm and a total laminar flow length of 60 mm, simultaneously unfolded, the two sides of the microtubule were insulated by 6 mm, and the rest was exposed outside the uniform wall to the surface temperature. The ratio of conductivity (ksf = 2.26–646). Ratio of microtubule thickness to inner radius is δ/Ri = 1, 10 and Re = 100, 500. Their results show that for thin walls, in addition to very low conductivity, the average Nusselt number is lower for thick walls. Cole and Cetin [26] investigated the conjugate heat transfer in heated microtubules produced by simulating Joule heating with electric current. A uniform heat source is generated within the wall and converted into a liquid with constant physical properties through a convection process. The differential equations of the model are analyzed and integrated using Green's function method. They also discussed the axial conduction effect of the wall on the temperature distribution.

In the present work, forced convective heat transfer in laminar flow in circular cross-section microtubules is predicted. Its walls are exposed to constant temperature in the normal flow direction of the fluid. Numerical results can be easily calculated using commercial CFD software packages and show the effect of different wall thicknesses, thermal conductivity, and Reynolds number on the thermal performance and average Nusselt number.

2 Model description and numerical analysis

Two-dimensional cylindrical coordinates simultaneously develop laminar flow, incompressibility, slip flow, steady state, constant solid–liquid physical properties, no internal dissipation, axisymmetric circular cross-section microtubules, and conjugation problems. The outer surface of the wall is exposed to a constant temperature along its entire length. The cross-section of the opposite solid face of the microtubule is insulating. The center of the microtubule is the axis of symmetry of the numerical model, as shown in Figure 1. Steady flow enters the microtubule at a velocity (u_{in}) and a constant temperature (T_∞).

2.1 Mesh independent

Mesh independence is important for high resolution results. The size (100 × 16), (200 × 20), (250 × 24), (300 × 32) and (350 × 36) affect Nusselt value. The liquid–solid wall interface in microtubules is independent of the mesh as shown in the table below. Note that the value of Nu number is approximately constant, so (300 × 32) was chosen to suit the case of the conjugate model.

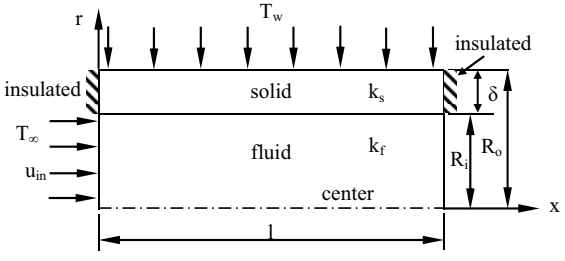

Figure 1: Geometry details, coordinate system, and boundary condition

Grid size	(100 × 16)	(200 × 20)	(250 × 24)	(300 × 32)	(350 × 36)
$\overline{Nu}$	3.9229	3.9319	3.9425	3.9603	3.9662

At micron flow, its properties are based on the Knudsen number (Kn = λ/Dh); the dimensionless number is the ratio of the molecular mean free path (λ) to a representative physical length scale (Dh). This can be the radius of the object [27].

Kn < 10^{-3} no slip flow.

10^{-3} < Kn < 10^{-1} slip flow.

10^{-1} < Kn < 10 transition flow.

Kn > 10 free – molecule flow.

The governing equations in this example are in addition to the continuity equation (1) and the fixed wall equation (5) [28].

1. Continuity equation

$$\frac{1}{r}\frac{\partial}{\partial r}(r \cdot v) + \frac{\partial u}{\partial x} = 0. \tag{1}$$

2. Momentum equation

in r-radial direction

$$\rho\left(v\frac{\partial v}{\partial r} + u\frac{\partial v}{\partial x}\right) = -\frac{\partial P}{\partial r} + \mu\left\{\frac{\partial}{\partial r}\left[\frac{1}{r}\frac{\partial}{\partial r}(r.\ v)\right] + \frac{\partial^2 v}{\partial x^2}\right\}. \tag{2}$$

In x-axial direction

$$\rho\left(v\frac{\partial u}{\partial r} + u\frac{\partial u}{\partial x}\right) = -\frac{\partial P}{\partial x} + \mu\left\{\frac{1}{r}\frac{\partial}{\partial r}\left[r\frac{\partial u}{\partial r}\right] + \frac{\partial^2 u}{\partial x^2}\right\}. \tag{3}$$

3. Energy equation

$$\rho.\ c_p\left(v\frac{\partial T_f}{\partial r} + u\frac{\partial T_f}{\partial x}\right) = k\left\{\frac{1}{r}\frac{\partial}{\partial r}\left[r\frac{\partial T_f}{\partial r}\right] + \frac{\partial^2 T_f}{\partial x^2}\right\}. \tag{4}$$

For the solid wall [16]

$$\frac{\partial^2 T_s}{\partial r^2} + \frac{1}{r}\frac{\partial T_s}{\partial r} + \frac{\partial^2 T_s}{\partial x^2} = 0. \tag{5}$$

The dimensionless term that is used in calculations and results [29]

$$k_{sf} = \frac{k_s}{k_f} \quad x\star = \frac{x}{\mathrm{Pr}\,\mathrm{Re}\,D_i},$$

$$T_{wi} = \frac{T - T_\infty}{T_w - T_\infty} \quad \mathrm{Re} = \frac{\rho u_{in} D_i}{\mu},$$

$$\mathrm{Pe} = \mathrm{Pr}\,\mathrm{Re} \quad \overline{\mathrm{Nu}} = \int_0^1 \mathrm{Nu}\,\mathrm{d}x.$$

The governing equations were numerically solved using finite volume techniques and the Fluent software CFD package. The model mesh is then generated using another software in Watch Fluent called GAMBIT, the problem is solved using this or more meshes, and the result is obtained by integrating the generalized equations. The lattice structure consists of a regular quadrilateral or rectangle with 6,600 cells and 7,300 nodes. Process six lattice patterns in one delimited file, each with different dimensions (δ/Ri = 0.25, 0.5, 0.75, 1, 1.25, and 1.5) according to wall thickness to microtubule inner diameter. The small area of the solid wall relative to the liquid area increases the Delta/Ri ratio until the concrete wall is larger than the liquid area.

Compared with ref. [21], the result of verification of Fluent is shown in Figure 2. When Re = 50, Pr = 1, ksf = 1, and δ/Ri = 0.08, the ratio of the dimensionless inner wall temperature (T_{wi}) to the dimensionless axial coordinate (x/RiRePr) has a proper identity and good consistency.

3 Results and discussion

Figures 3–8 plotted the dimensionless temperature of the inner wall of the microtubule, the flow axis divided by the size of (RePrDi). The purpose of this quantity is to determine the hot inlet length, and its value is calculated from equation (6) [30] given below; therefore, the value of x^* is equal to 0.055, representing the end of the hot inlet length. Six Figures 3–8 can be clearly observed, each with five graphs (a, b, c, d, and e) representing different states of Reynolds number (Re = 200, 400, 600, 800, and 1,000), the x^* value at the end of the tube varies from chart to chart. This means that the heat flow has reached full flow, but this is only one note in the first number with (Re = 200), and the other four have no full heat flow because x^* is less than 0.05. Note that the value of the wall thickness to inner diameter ratio ksf plays a crucial role in the temperature distribution. If its value is high, it means that the thermal conductivity of the wall will increase and the thermal resistance will decrease. The temperature of the inner wall surface is similar to its outer surface. That is how Figures 3–8 notice it and show an increase in T_{wi} with an increase in ksf for each range mentioned (ksf = 1, 2, 3, 4, and 5). Figures 3–8 generally show that increasing the δ/Ri ratio leads to a decrease in T_{wi}. This is due to the increase in the axial heat conduction of the wall and the decrease in the thermal resistance of the wall. Figure (3a) shows the range from higher values (such as T_{wi} = 0.94) to the minimum of different ksf ratios (such as T_{wi} = 0.78) to the maximum found in Figure (8a) above range (T_{wi} = 0.74) and lowest value (T_{wi} = 0.35). Furthermore, the unquoted numbers decrease with the increase in the δ/Ri ratios, but there is a difference between the highest and lowest values. However, it has the same behavior. Note that the charts (3–8) each contain five charts, numbered a–e, with value differences (Re = 200, 400, 600, 800, and 1,000). These numbers have the same (δ/Ri) ratio. It can be noted the effect of Reynolds number on T_{wi} behavior and whether there is an inverse relationship between them.

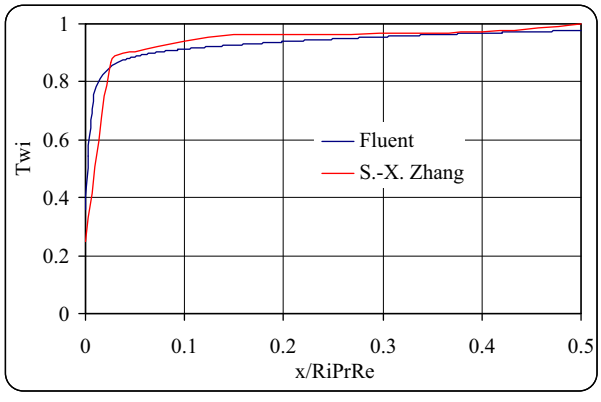

Figure 2: Dimensionless wall temperature (T_{wi}) with non-dimensional axial coordinate for the case is: Pr = 1, Re = 50, δ/Ri = 0.08, and ksf = 1.

For example, in the case of Figure 3 (δ/Ri = 0.25), by increasing the five plots of Re (a, b, c, d, and e), the curve tends to decrease but is ineffective, while in Figure 4 the values start to move away from plot 3 and further declines.

The average Nusselt number increases as the Reynolds number increases, as shown in Figure 9, as the velocity of the fluid increases. Therefore, the fluid transfers more heat through the molecules of the solid–liquid interface line. Furthermore, an increase in the Reynolds number leads to an increase in the inlet length; the local Nusselt number in this region is always high; after this region, its value decreases and remains constant and lower due to the fully developed heat of the flow. From Figure 9, this value of the average Nusselt number is the maximum at ksf = 1, and then its value decreases as ksf increases, considering that ksf is the ratio of the thermal conductivity of the wall to the liquid, compared to that of the liquid, thermal conductivity is constant independent of ksf, so increasing ksf means increasing ksf only if the wall thickness (δ) is still constant in each case.

Increasing the ratio of the ksf of conduction to axial wall conduction will increase due to the reduction in thermal resistance through the microtube wall, thereby

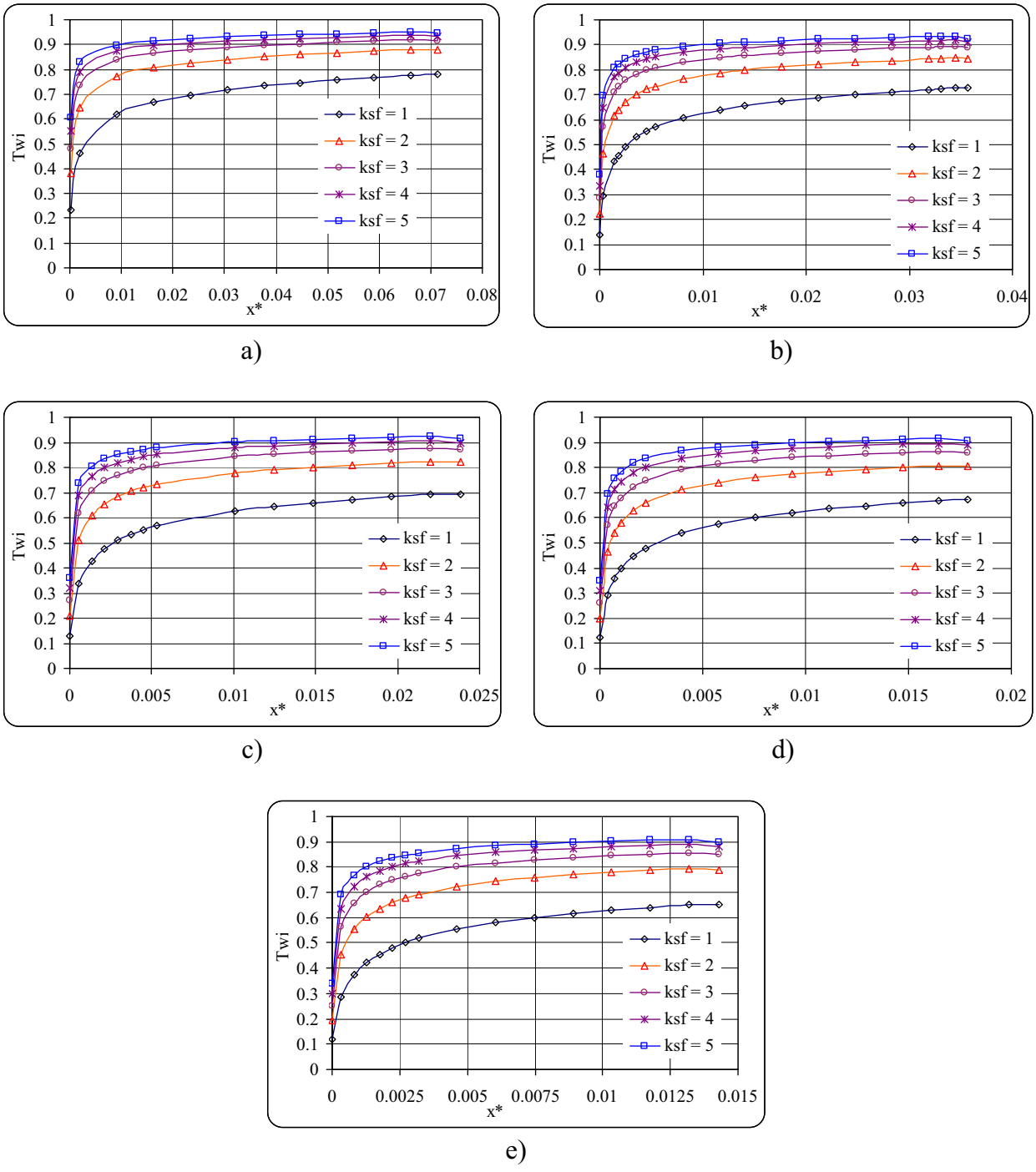

Figure 3: Relationship between dimensionless inside wall temperature vs dimensionless axial coordinate $\delta/R_i = 0.25$ and Pr = 7, with variable ksf ratio. (a) Re = 200, (b) Re = 400, (c) Re = 600, (d) Re = 800, and (e) Re = 1,000.

increasing the heat transfer cross-section of the wall in the axial direction; this effect results in high heat transfer in conduction and therefore in fluid. The high radial heat transfer in the direction leads to a high value of the convection coefficient (h) according to equation (6). This coefficient is proportional to the average Nusselt number of equation (7), and its value depends on (h) in the calculation.

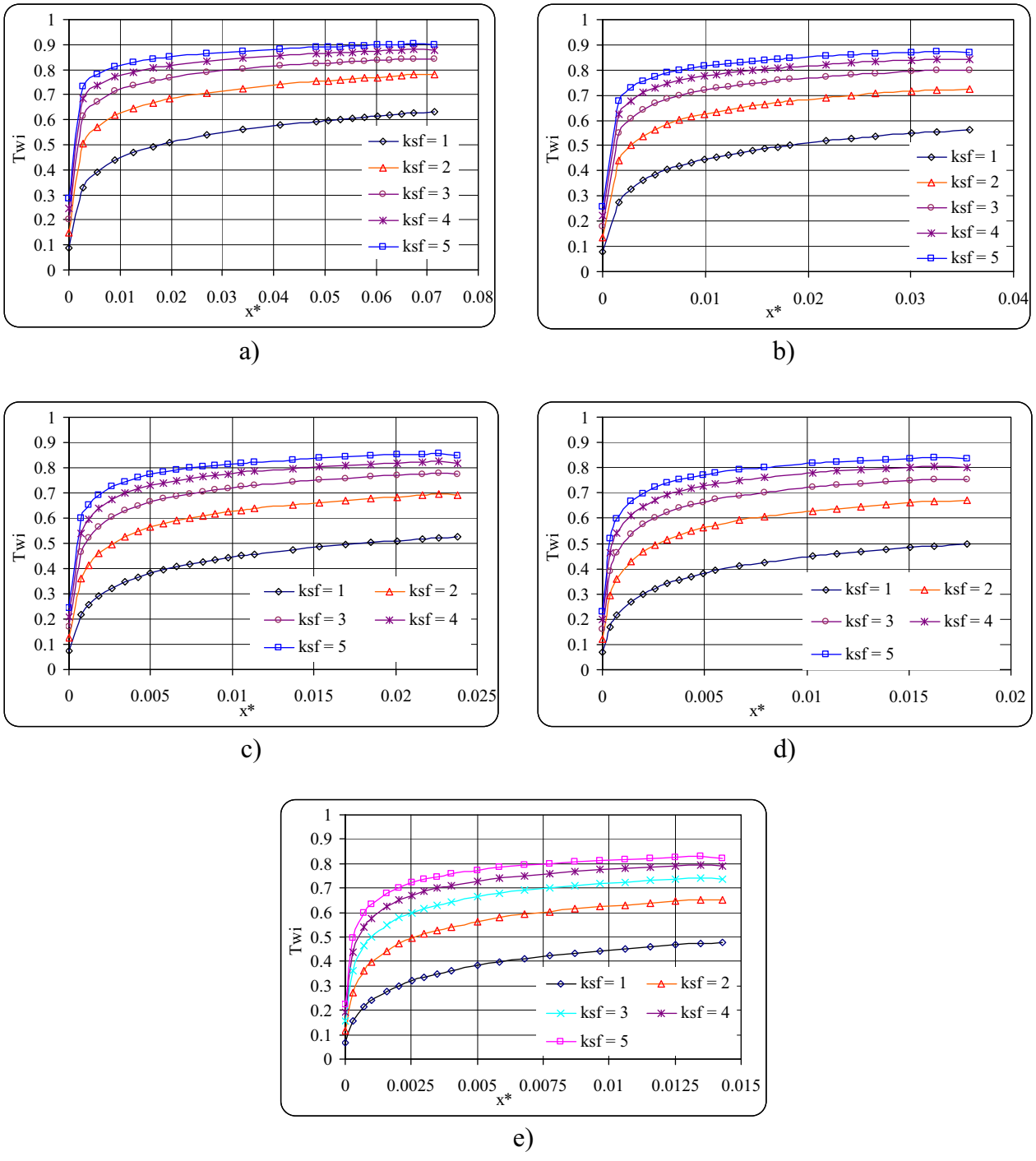

Figure 4: Relationship between dimensionless inside wall temperature vs dimensionless axial coordinate $\delta/R_i = 0.5$ and Pr = 7, with variable ksf ratio. (a) Re = 200, (b) Re = 400, (c) Re = 600, (d) Re = 800, and (e) Re = 1,000.

$$h = \frac{q''_{wi}}{T_{wi} - T_{fb}}, \tag{6}$$

$$\mathrm{Nu} = \frac{hD_i}{k_f}. \tag{7}$$

From Figure 9, it can be seen that for each value of ksf and Reynolds number, the average Nusselt number increases as the δ/Ri ratio increases. This effect leads to an increase in wall thickness, while the radius of the microtubule remains constant, an increase in δ/Ri means an increase in wall thickness, which results in an

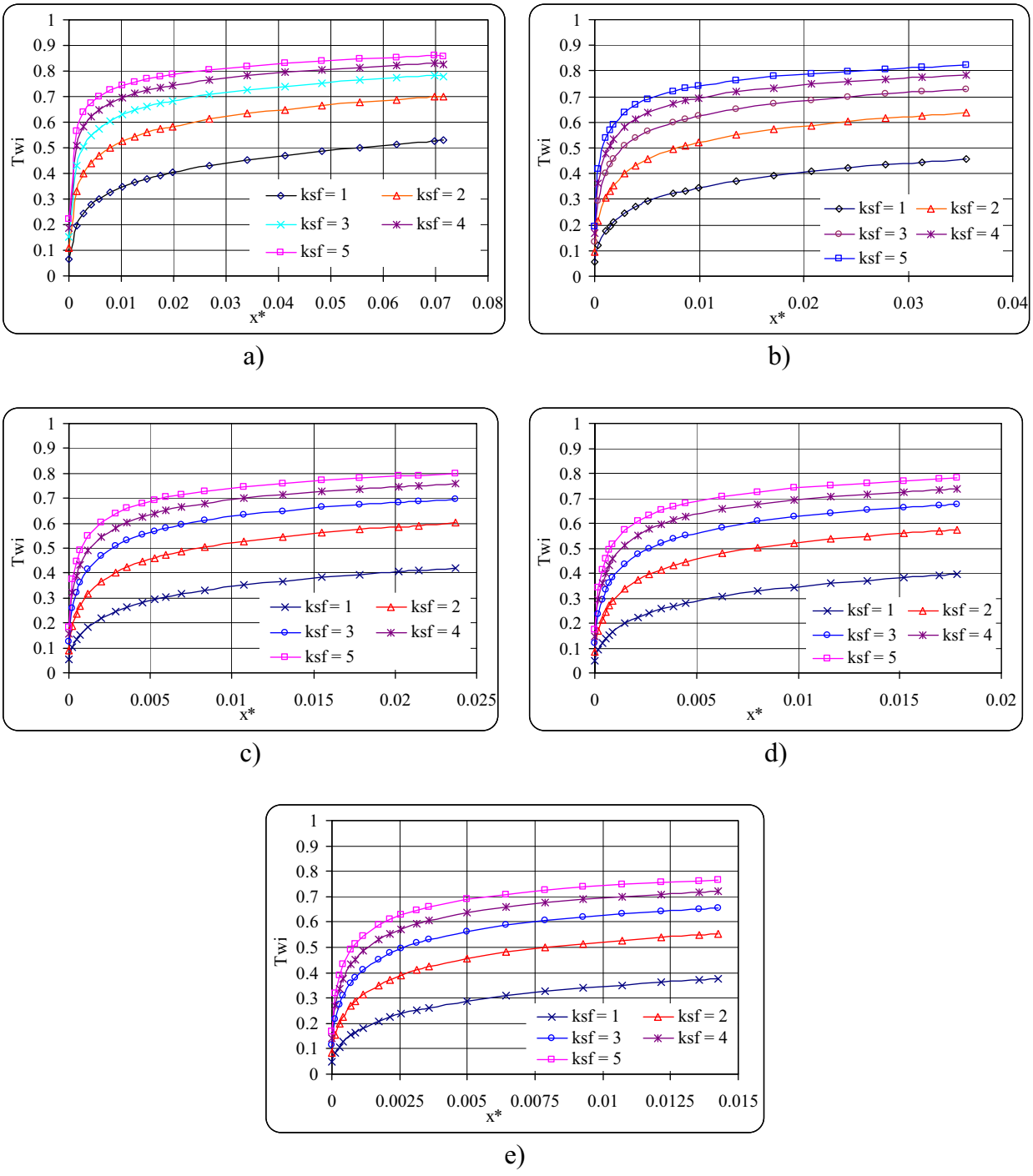

Figure 5: Relationship between dimensionless inside wall temperature vs dimensionless axial coordinate $\delta/R_i = 0.75$ and Pr = 7, with variable ksf ratio. (a) Re = 200, (b) Re = 400, (c) Re = 600, (d) Re = 800, and (e) Re = 1,000.

increase in the transmission cross-sectional area of the microtubule parallel to Fourier's law in fluid flow of axial tube heat. Increasing the cross-sectional area reduces thermal resistance, while increasing axial heat transfer towards the tube ends increases the fluid temperature and thus the convective heat transfer coefficient. Therefore, as the wall thickness increases, the average Nusselt number will be higher.

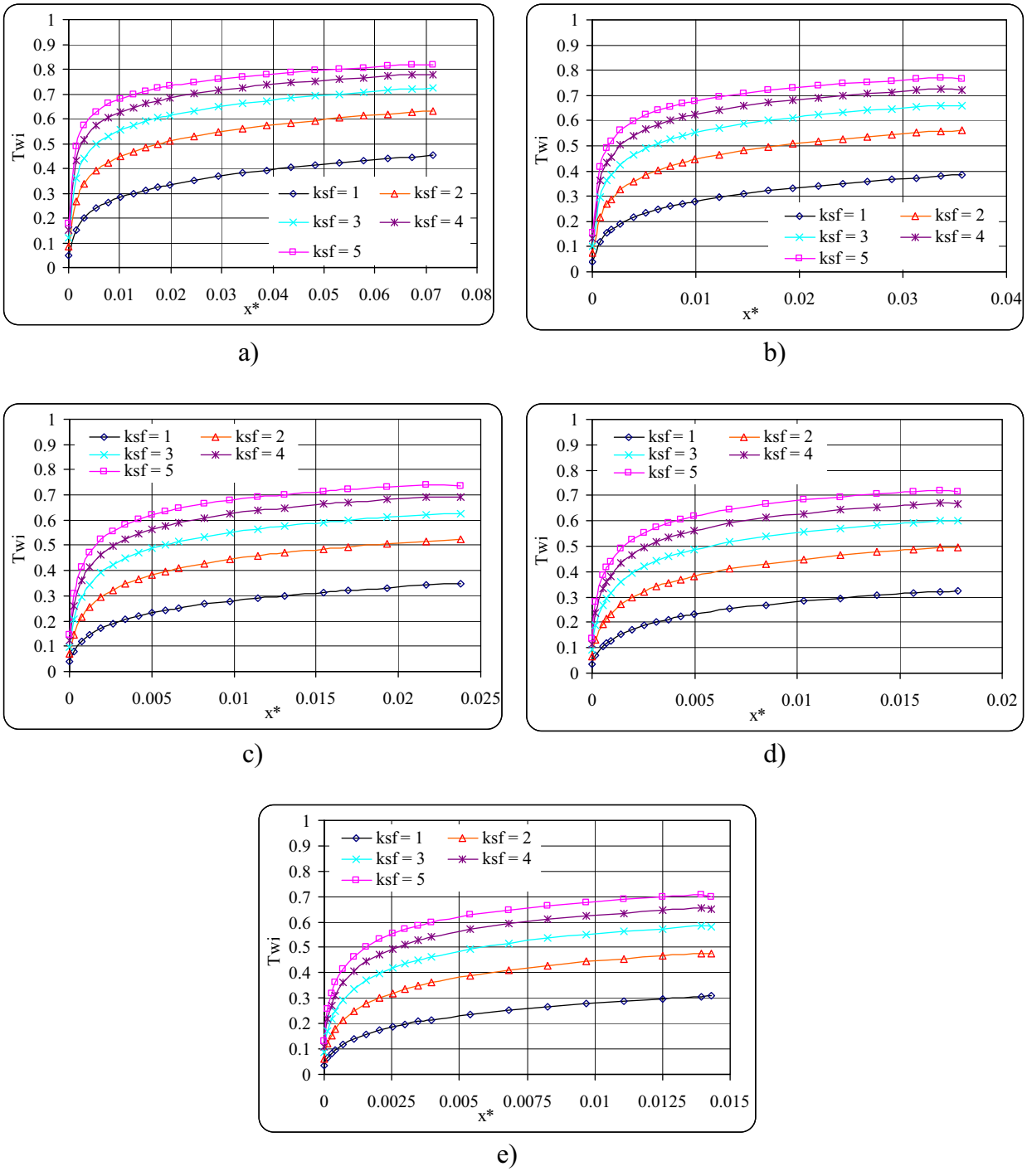

Figure 6: Relationship between dimensionless inside wall temperature vs dimensionless axial coordinate $\delta/R_i = 1$ and Pr = 7, with variable ksf ratio. (a) Re = 200, (b) Re = 400, (c) Re = 600, (d) Re = 800, and (e) Re = 1,000.

4 Conclusion

The results of the work were numerically analyzed by Fluent software, and the flow in the microtubules was presented in digital form. Static, incompressible, conjugate, and laminar flow simultaneously evolve and predict the following:

1. The increment of the T_{wi} value to the ksf value within the specified range included in the study.
2. The decrease in the value of T_{wi} is due to the increase in the ratio of δ/Ri in the given range.
3. An increase in the Reynolds number leads to a decrease in the T_{wi} value, which becomes more pronounced with an increase in δ/Ri.

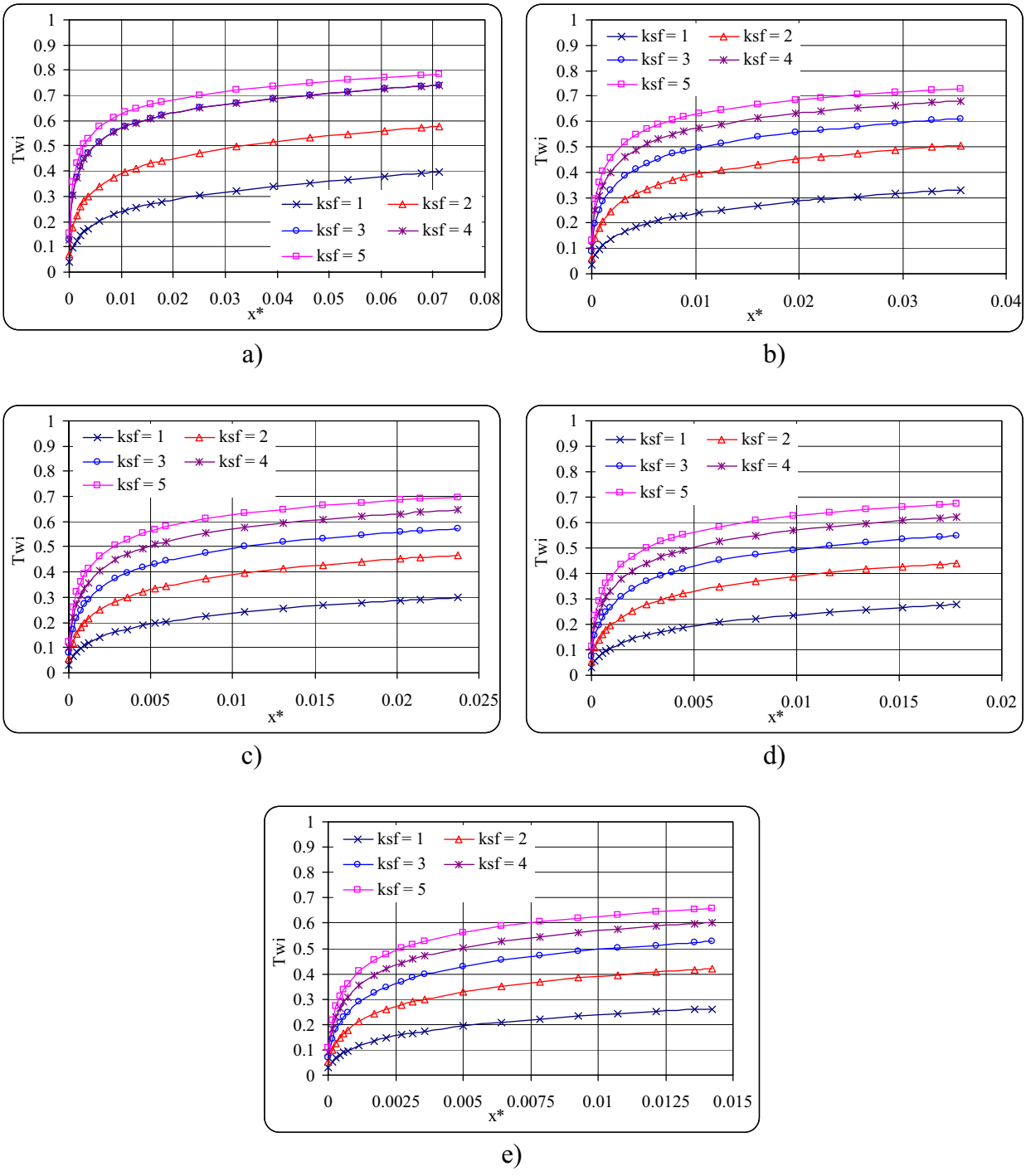

Figure 7: Relationship between dimensionless inside wall temperature vs dimensionless axial coordinate $\delta/R_i = 1.25$ and Pr = 7, with variable ksf ratio. (a) Re = 200, (b) Re = 400, (c) Re = 600, (d) Re = 800, and (e) Re = 1,000.

4. The average Nusselt number increases with the Reynolds number within the range suggested by the study.
5. An increase in the thermal conductivity of the micro-tubular material or an increase in the ksf ratio results in a decrease in the value of the mean Nusselt number within the range suggested by the study.
6. An increase in microtubule thickness or an increase in the δ/Ri ratio increases the average Nusselt number within the interval specified for the δ/Ri value in the study.

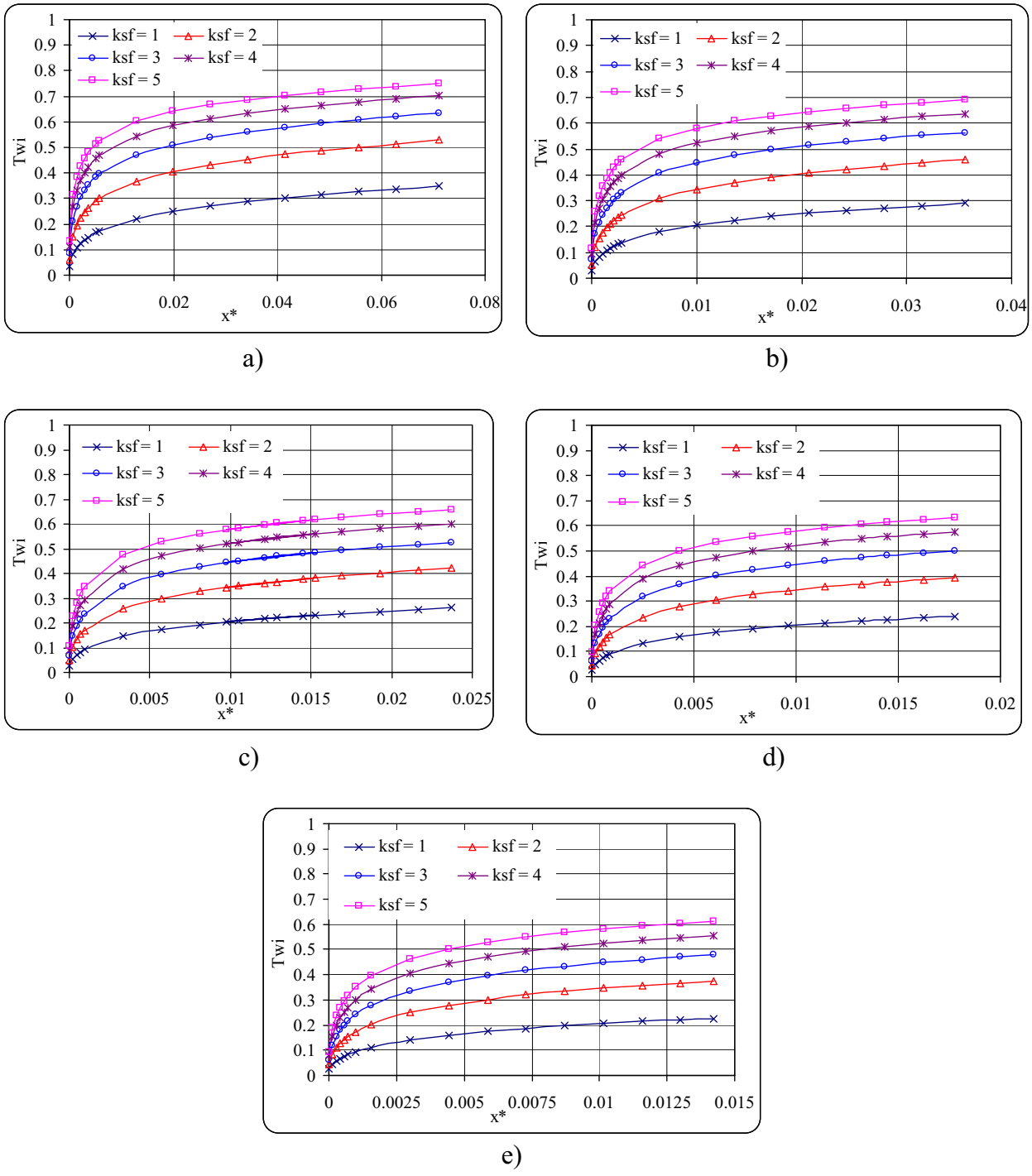

Figure 8: Relationship between dimensionless inside wall temperature vs dimensionless axial coordinate $\delta/R_i = 1.5$ and Pr = 7, with variable ksf ratio. (a) Re = 200, (b) Re = 400, (c) Re = 600, (d) Re = 800, and (e) Re = 1,000.

Nomenclature

C_p	specific heat of fluid (J/kg K^{-1})
D_i	inside diameter of microtube (μm)
D_o	outside diameter of microtube (μm)
h	convective heat transfer coefficient (W/m^{2}K^{-1})
k_f	fluid thermal conductivity (W/m K^{-1})
k_s	solid thermal conductivity (W/m K^{-1})
ksf	wall to fluid thermal conductivity ratio
l	total length of microtube (μm)
L_{th}	thermal entrance length (μm)
Nu	local Nusselt number

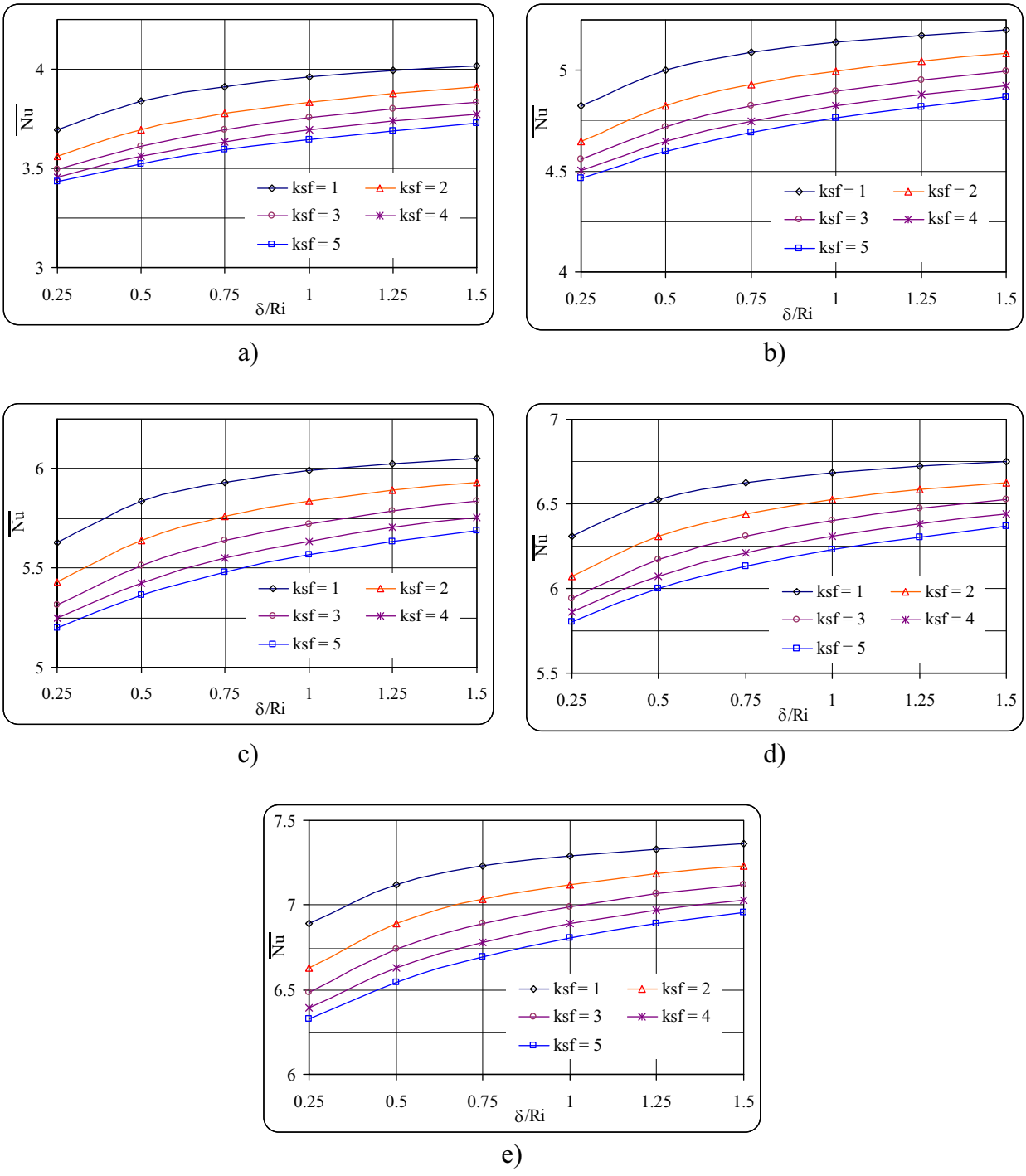

Figure 9: Average Nusselt number vs wall thickness to inside radius ratio with variable ksf ratio. (a) Re = 200, (b) Re = 400, (c) Re = 600, (d) Re = 800, and (e) Re = 1,000.

$\overline{\mathrm{Nu}}$	average Nusselt number
Pr	Prandtl number
Pe	Peclet number
P	pressure (N/m^2)
q''_{wi}	inside wall heat flux (W/m^2)
r	radial coordinate (m)
R_i	inside wall radius (m)
R_o	outside radius (m)
Re	Reynolds number
T_s	solid temperature (K)
T_f	fluid temperature (K)
T_{fb}	fluid bulk temperature (K)

T_{wi} dimensionless inside wall temperature
T_{∞} inlet temperature (K)
T_{w} outside wall temperature (K)
u axial direction velocity (m/s)
u_{in} inlet velocity (m/s)
v radial direction velocity (m/s)
x axial coordinate (m)
$x^{\star}$ dimensionless axial coordinate

Greek symbol

δ thickness of microtube wall (μm)
ρ fluid density (kg/m^3)
μ dynamic viscosity (Pa s)

Acknowledgments: The authors would like to express their gratitude to the Al-Mustaqbal University college for their financial support of project.

Conflict of interest: Authors state no conflict of interest.

References

[1] Smaisim GF, Abdulhadi AM, Uktamov KF, Alsultany FH, Izzat SE, Ansari MJ, et al. Nano fluids: Properties and applications. J Sol–Gel Sci Technol. 2022;102(3):1–35.
[2] Alharbi KA, Smaisim GF, Sajadi SM, Fagiy MA, Aybar HŞ, Elkhatib SE. Numerical study of lozenge, triangular and rectangular arrangements of lithium-ion batteries in their thermal management in a cooled-air cooling system. J Energy Storage. 15 August 2022;52(Part B):104786. doi: 10.1016/j.est.2022.104786.
[3] Tian MW, Smaisim GF, Yan SR, Sajadi SM, Mahmoud MZ, Aybar HŞ, et al. Economic cost and efficiency analysis of a lithium-ion battery pack with the circular and elliptical cavities filled with phase change materials. J Energy Storage. 15 August 2022;52(Part B):104794. doi: 10.1016/j.est.2022.104794.
[4] Wu W, Smaisim GF, Sajadi SM, Fagiry MA, Li Z, Shamseldin MA, et al. Impact of phase change material-based heatsinks on lithium-ion battery thermal management: A comprehensive review. J Energy Storage. 15 August 2022;52(Part B):104874. doi: 10.1016/j.est.2022.104874.
[5] AbdulHussein WA, Abed AM, Mohammed DB, Smaisim GF, Baghaei S. Investigation of boiling process of different fluids in microchannels and nanochannels in the presence of external electric field and external magnetic field using molecular dynamics simulation. Case Stud Therm Eng. July 2022;35:102105. doi: 10.1016/j.csite.2022.102105.
[6] Smaisim GF, Prabu NM, Senthilkumar AP, Abed AM. Synthesis of biodiesel from fish processing waste by nano magnetic catalyst and its thermodynamic analysis. Case Stud Therm Eng. 2022;35:102115.
[7] Mozafarifard M, Azimi A, Sobhani H, Smaisim GF, Toghraie D, Rahmani M. Numerical study of anomalous heat conduction in absorber plate of a solar collector using time-fractional single-phase-lag model. Case Stud Therm Eng. June 2022;34:102071. doi: 10.1016/j.csite.2022.102071.
[8] Al-Abadi AK, Kridi AF, Hussain GF. Comparison between simulated and calculated power of the solar chimney with black concrete base using ANSYS program. Al-Qadisiya J Eng Sci. 2010;3(3):347–64.
[9] Al-Madhhachi H, Smaisim GF. Experimental and numerical investigations with environmental impacts of affordable square pyramid solar still. Sol Energy. 2021;216:303–14.
[10] Lefteh A, Houshmand M, Khorrampanah M, Smaisim GF. Optimization of modified adaptive neuro-fuzzy inference system (MANFIS) with artificial bee colony (ABC) algorithm for classification of bone cancer. 2022 Second International Conference on Distributed Computing and High Performance Computing (DCHPC); 2022. pp. 78–81. doi: 10.1109/DCHPC55044.2022.9731840.
[11] Sallal AS, Smaisim GF, Thahab SM. The heat transfer from fined perforated pipe improved due to nano-fluid. J Phys Conf Ser. August 2021, 1973(1):012075. doi: 10.1088/1742-6596/1973/1/012075. Al-Mustaqbal University College, Babylon Iraq.
[12] Smaisim GF. Enhancement heat transfer of cu-water nano-fluids with thermophysical properties modeling by artificial neural network. J Babylon Univ Eng Sci. 2017;25(5):1721–35
[13] Barozzi GS, Pagliarini G. A method to solve conjugate heat transfer problems: the case of fully developed laminar flow in a pipe. J Heat Transf. Feb. 1985;107(1):77–83 (7 Pages).
[14] Celata GP, Cumo M, Marconi V, McPhail SJ, Zummo G. Microtube liquid single-phase heat transfer in laminar flow. Int J Heat Mass Transf. 2006;49:3538–46.
[15] Lelea D, Cioabla A, Laza I, Mihon L. The Nu number behavior on micro-tube heat transfer and fluid flow of dielectric fluid. Open Thermodyn J. 2009;3:38–41.
[16] Zhang SX, He YL, Lauriat G, Tao WQ. Numerical studies of simultaneously developing laminar flow and heat transfer in microtubes with thick wall and constant outside wall temperature. Int J Heat Mass Transf. 2010;53:3977–89.
[17] Girgin I, Turker M. Axial heat conduction in laminar duct flows. J Nav Sci Eng. 2011;7(2):30–45.
[18] Elmarghany MR, Mansour MH, Sultan AA, Sabry MN. Modeling of Conjugate Heat Transfer. Mansoura Eng J. March (2016);41(1):16–23.
[19] Chandel S, Misal RD, Beka YG. Convective heat transfer through thick-walled pipe. Int Conf Model Optim Comput Procedia Eng. 2012;38:405–11.
[20] Lin TY, Kandlikar SG. A theoretical model for axial heat conduction effects during single-phase flow in microchannels. J Heat Transf. Copyright 2012 by ASME February 2012;134:020902-1.
[21] Rahimi M, Mehryar R. Numerical study of axial heat conduction effects on the local nusselt number at the entrance and ending regions of a circular microchannel. Int J Therm Sci. 2012;59:87–94.
[22] Moharana MK, Singh PK, Khandekar S. Optimum nusselt number for simultaneously developing internal flow under conjugate conditions in a square microchannel. J Heat Transf. Copyright 2012 By ASME July 2012;134:071703-1.
[23] Astaraki MR, Tabari NG. Two-dimensional analytical solution of the laminar forced convection in a circular duct with periodic

boundary condition. Hindawi Publishing Corporation J Thermodyn. 2012;2012:8793906.
[24] Touahri S, Boufendi T. Numerical study of the conjugate heat transfer in a horizontal pipe heated by Joulean effect. Therm Sci. Year 2012;16(1):53–67.
[25] Kumar M, Maharana MK. Axial wall conduction in partially heated microtubes. Proceedings of The 22nd National And 11th International, ISHMT-ASME Heat And Mass Transfer Conference. India: IIT Kharagpur; December 28–31 2013.
[26] Cole K, Cetin B. Modeling of conjugate heat transfer in an electrically heated microtube. Istanbul: 8th ICCHMT; 25–28 May 2015.
[27] Kostikov YA. Alexander Mikhailovich Romanenkov, approximation of the multidimensional optimal control problem for the heat equation (applicable to computational fluid dynamics (CFD)). Civ Eng J. April 2020;6(4):743–68.
[28] Al-Maliky RF. Force convection of laminar liquid flow inside pipe exerted to non-uniform heat flux. Int J Therm Technol. 2013;3(3):113–19.
[29] Adeyemi TS. Analytical solution of unsteady-state Forchheimer flow problem in an infinite reservoir: the Boltzmann transform approach. J Hum Earth Future. 2021;2(3):225–33.
[30] Han J-C, Wright LM. Heat Conduction Equations. Analytical Heat Transfer. 2002;1–874.